A second-order numerical scheme for the porous shallow water equations based on a DOT ADER augmented Riemann solver

A second-order numerical scheme for the porous Shallow Water Equations based on a DOT ADER augmented Riemann solver

Alessia Ferrari[a,*], Renato Vacondio[a], Paolo Mignosa[a]

[a]*Department of Engineering and Architecture, University of Parma, Parco Area delle Scienze 181/A, 43124 Parma, Italy*

Abstract

In the present work, a novel DOT ADER numerical solver capable of handling porosity and bottom discontinuities in the framework of the 1D porous Shallow Water Equations (SWEs) is presented. In order to ensure the preservation of the water at rest condition, a new set of well-balanced governing equations based on the isotropic porosity parameter is derived. The effects exerted by the bed slope and porosity variation source terms are accurately accounted for inside the Riemann solver: to this purpose, an augmented Riemann problem is created by adding two fictitious equations stating the invariance of porosity and bottom in time to the SWEs system. With the aim of computing the non-conservative fluxes, which in the augmented system replace the original source terms, meanwhile ensuring robustness, stability and accuracy, a novel approximate numerical scheme, based on the entropy-satisfying DOT family, is introduced. The extension of the novel Riemann solver, which strictly conserves mass, to a second order of accuracy in both space and time is addressed in the ADER framework. The fulfillment of the *C-property* condition (i.e. the exact preservation of an initial quiescent flow) in the presence of a discontinuous porosity field and over a non-flat bottom with abrupt variation is theoretically proved and numerically verified. The capability of the proposed numerical scheme to

*Corresponding author

Email address: alessia.ferrari@unipr.it (Alessia Ferrari)

simulate some Riemann problems developing across porosity discontinuities and bed steps is finally assessed.
Keywords: Shallow Water Equations with porosity, Augmented Riemann problems, DOT, ADER, Porosity discontinuity, Bed step

---

1. Introduction

The modeling of flooding events in urban areas represents a crucial task dealing with hazard and risk assessment. In this framework, the Shallow Water Equations (SWEs) with porosity are a promising tool to account for the effects exerted by buildings, without impacting on the mesh resolution and hence on the computational times. In fact, the storage isotropic porosity is defined as the volume fraction of the urban area available for mass and momentum storage; Defina et al. (1994) firstly introduced this concept in the SWEs to deal with partially dry areas.

Since then, several differential isotropic formulations have been presented in order to consider both the reduced storage and the additional resistances that buildings exert on the flow: Guinot & Soares-Frazão (2006), Soares-Frazão et al. (2008), Cea & Vázquez-Cendón (2010), Finaud-Guyot et al. (2010), Benkhaldoun et al. (2016), Ferrari et al. (2017), Velickovic et al. (2017), Cozzolino et al. (2018), Ferrari et al. (2019), Viero (2019).

Other works derived the equations in integral form and adopted, additionally to the storage porosity, a conveyance parameter to account for the connectivity of the urban medium: Sanders et al. (2008), Özgen et al. (2016a), Özgen et al. (2016b), Bruwier et al. (2017), Guinot et al. (2017), Guinot et al. (2018).

Since porosity schemes aim at simulating flood events on real urban layouts, beyond the formulation derivation and the chosen porosity parameter, the free-surface modeling has to ensure a stable treatment of discontinuities that are commonly present in porous fields and bathymetries.

An accurate way to fix this issue is to account for the effects of the source terms inside the Riemann solver creating an augmented Riemann problem,

where the variables appearing in the source terms are added to the list of the conserved variables, and the source terms are substituted by non-conservative fluxes. In this framework, some works focused on the bed slope source term: Bernetti et al. (2008), George (2008), Murillo & García-Navarro (2010), Rosatti & Begnudelli (2010), Cozzolino et al. (2011), Murillo & García-Navarro (2012), Navas-Montilla & Murillo (2015), Caleffi et al. (2016), among others. With regard to the treatment of the porosity source term by means of augmented Riemann problems, Benkhaldoun et al. (2016) proposed a nonhomogeneous solver based on a predictor-corrector procedure for unstructured triangular grids, whereas Ferrari et al. (2017) derived an augmented 2D Roe solver capable of handling porous abrupt variations on Cartesian grids. The scheme of Ferrari et al. (2017) was developed according to some physical assumptions concerning the porosity variation and neglecting the bottom reaction. Moreover, dealing with a Roe scheme, an entropy-fix procedure was required. Furthermore, that scheme did not exactly preserve the condition of quiescent flow (as the adopted governing equations did not inherently guarantee this condition), and finally it was limited to first order of accuracy.

This paper aims at deriving, in a 1D framework, a novel high-order approximate Riemann solver capable of treating porous and bottom jumps, meanwhile ensuring the exact preservation of the water at rest condition. To this purpose, a new set of well-balanced governing equations, based on the isotropic porosity parameter, is derived, and an augmented Riemann solver is created to solve these non-conservative equations. A novel numerical solver, based on the path-conservative DOT (Dumbser & Toro (2011)) scheme, is developed in order to obtain a robust, general and entropy-satisfying approximate Riemann solver, capable of treating the non-conservative products (due to porosity discontinuities and bed steps), without requiring computationally expensive entropy-fix procedure typical of the Roe-based ones. The numerical scheme is then extended to second order following the ADER approach (Toro et al. (2001), Titarev & Toro (2002), Toro & Titarev (2002)).

The reminder of the paper is organized as follows: in Section 2 the new set

of the well-balanced governing equations is derived. Section 3 is dedicated to the augmented Riemann problem definition and to the study of its eigenstructure. The first order DOT numerical solver is described in Section 4, meanwhile the extension to the second-order in the framework of the ADER approach is described in Section 5. In Section 6, the exact preservation of the water at rest condition is theoretically proved and numerically verified. Then, the DOT-ADER solver is applied to test the order of convergence and to simulate some Riemann problems developing across porosity discontinuities and bed steps in Section 7. Finally, the conclusions of the work and insights into the future developments are outlined in Section 8.

2. Governing equations

In this work, the original formulation of the 2D-SWEs with a single storage porosity parameter (Guinot & Soares-Frazão (2006)) is considered. Assuming a frictionless bed, and neglecting the head loss terms due to obstructions, in a 1D framework, the governing equations written in conservation form become:

$$\begin{cases} \frac{\partial \phi h}{\partial t} + \frac{\partial \phi uh}{\partial x} = 0 \\ \frac{\partial \phi uh}{\partial t} + \frac{\partial}{\partial x}(\phi u^2 h + \frac{1}{2} g \phi h^2) = \frac{1}{2} g h^2 \frac{\partial \phi}{\partial x} - g \phi h \frac{\partial z}{\partial x} \end{cases} \tag{1}$$

where h represents the water depth, ϕ the porosity, u the velocity, g the gravitational acceleration, and z the bottom elevation. The source terms at the right hand of the momentum equation represent the reaction due to the porosity variation (first term) and to the bed slope (second term), respectively.

With the aim of obtaining a well-balanced scheme, and following the idea originally proposed by Liang & Borthwick (2009) for the classical SWEs, the water depth h in system (1) is substituted by the water surface elevation η, recalling that $\eta = h + z$:

$$\begin{cases} \frac{\partial \phi(\eta - z)}{\partial t} + \frac{\partial \phi uh}{\partial x} = 0 \\ \frac{\partial \phi uh}{\partial t} + \frac{\partial}{\partial x}[\phi u^2 h + \frac{1}{2} g \phi \left(\eta^2 - 2\eta z + z^2\right)] = \frac{1}{2} g h^2 \frac{\partial \phi}{\partial x} - g \phi h \frac{\partial z}{\partial x} \end{cases} \tag{2}$$

Then, considering both porosity and bottom variables constant in time, after simple manipulations, the new set of the governing equations results:

$$\begin{cases} \frac{\partial \phi\eta}{\partial t} + \frac{\partial \phi uh}{\partial x} = 0 \\ \frac{\partial \phi uh}{\partial t} + \frac{\partial}{\partial x}\left[\phi u^2 h + \frac{1}{2} g\phi(\eta^2 - 2\eta z)\right] = \frac{1}{2} g(\eta^2 - 2\eta z)\frac{\partial \phi}{\partial x} - g\phi\eta\frac{\partial z}{\partial x} \end{cases} \tag{3}$$

As will be theoretically proved and numerically verified in Section 6, system (3) guarantees the *C-property* (i.e. the exact preservation of the water at rest condition).

3. The mathematical model

With the aim of taking into account the effects of both porosity and bed elevation discontinuities inside the Riemann solver, ϕ and z are considered as additional fictitious conserved variables (as the original idea of LeRoux (1998) for the bed slope term). This means that two equations stating the invariance of porosity and bed elevation in time are added to system (3), resulting in the following augmented Riemann problem written in compact form:

$$\frac{\partial \mathbf{U}}{\partial t} + \frac{\partial \mathbf{F}}{\partial x} + \mathbf{H}\frac{\partial \mathbf{U}}{\partial x} = 0 \tag{4}$$

where the vectors of the conserved variables $\mathbf{U}$ and of the fluxes $\mathbf{F}$, and the matrix of the non-conservative fluxes $\mathbf{H}$ originated by the non-conservative products, whose presence deserves special attention (Abgrall & Karni (2010)), are defined as:

$$\mathbf{U} = \begin{bmatrix} \phi\eta \\ \phi uh \\ \phi \\ z \end{bmatrix}, \mathbf{F} = \begin{bmatrix} \phi uh \\ \phi u^2 h + \frac{1}{2} g\phi(\eta^2 - 2\eta z) \\ 0 \\ 0 \end{bmatrix}, \mathbf{H} = \begin{bmatrix} 0 & 0 & 0 & 0 \\ 0 & 0 & -\frac{1}{2} g(\eta^2 - 2\eta z) & g\phi\eta \\ 0 & 0 & 0 & 0 \\ 0 & 0 & 0 & 0 \end{bmatrix} \tag{5}$$

The definition of the Generalized Riemann Problem in system (4) implies that the original source terms now influence the eigenstructure of the problem. Particularly, the eigenvalues and eigenvectors of the 1D porous SWEs in Eq. (1), which correspond to those of the classical SWEs (Guinot & Soares-Frazão

(2006)), may not coincide with those of system (4). In order to study the eigenstructure of the augmented problem, system (4) is rewritten in the following quasi-linear form:

$$\frac{\partial \mathbf{U}}{\partial t} + \mathbf{A}\frac{\partial \mathbf{U}}{\partial x} = 0 \tag{6}$$

where the matrix $\mathbf{A}$ represents the sum of the Jacobian matrix of the flux vector $\mathbf{F}$ and the non-conservative one $\mathbf{H}$:

$$\mathbf{A} = \frac{d\mathbf{F}}{d\mathbf{U}} + \mathbf{H} = \begin{bmatrix} 0 & 1 & 0 & 0 \\ gh - u^2 & 2u & u^2 z - g\eta^2 + g\eta z & u^2\phi \\ 0 & 0 & 0 & 0 \\ 0 & 0 & 0 & 0 \end{bmatrix} \tag{7}$$

The computation of the roots of the characteristic polynomial $|\mathbf{A} - \lambda\mathbf{I}| = 0$ (Toro (2001)) allows for the definition of the following eigenvalues $\lambda_1, \lambda_2, \lambda_3$, and λ_4:

$$\lambda_1 = u - \sqrt{gh},\ \lambda_2 = 0,\ \lambda_3 = 0,\ \lambda_4 = u + \sqrt{gh} \tag{8}$$

Since the eigenvalues are real and distinct the augmented system (4) is hyperbolic (even if not stricly hyperbolic). The characteristic fields λ_1 and λ_4, which correspond to those of the SWEs without porosity, are genuinely nonlinear, and they are associated with rarefactions and shocks, while λ_2 and λ_3 are linearly degenerate and they are associated with contact waves.

Once the eigenvalues are defined, the right eigenvectors are calculated according to the relation $\mathbf{AR}{=}\lambda\mathbf{R}$ (Toro (2001)) that associates a given eigenvector $\mathbf{R}$ to each eigenvalue λ of matrix $\mathbf{A}$. Thus, the set of the right eigenvectors results:

$$\mathbf{R}_1 = \begin{bmatrix} 1 \\ u - \sqrt{gh} \\ 0 \\ 0 \end{bmatrix}, \mathbf{R}_2 = \begin{bmatrix} \frac{-u^2 z + g\eta^2 - g\eta z}{gh - u^2} \\ 0 \\ 1 \\ 0 \end{bmatrix}, \mathbf{R}_3 = \begin{bmatrix} \frac{-u^2\phi}{gh - u^2} \\ 0 \\ 0 \\ 1 \end{bmatrix}, \mathbf{R}_4 = \begin{bmatrix} 1 \\ u + \sqrt{gh} \\ 0 \\ 0 \end{bmatrix} \tag{9}$$

4. The DOT Riemann Solver

Following the formalism of path-conservative schemes (Dal Maso et al. (1995), Parés (2006), Castro et al. (2007)), Dumbser & Toro (2011) extended the Osher-Solomon Riemann solver (Osher & Solomon (1982)) to non-conservative hyperbolic systems, leading to the DOT Riemann solver, which is robust, complete, and entropy-satisfiying. In the framework of finite-volume schemes, the spatial and temporal integration of Eq. (6) in the control volume $[x_{i-\frac{1}{2}}, x_{i+\frac{1}{2}}]\times[t^n, t^{n+1}]$ leads to the following formula for updating the solution to next time-step (Parés (2006), Castro et al. (2006), Canestrelli et al. (2009), Stecca et al. (2016)):

$$\mathbf{U}_i^{n+1} = \mathbf{U}_i^n - \frac{1}{\Delta x}\int_{t^n}^{t^{n+1}}\int_{x_{i-\frac{1}{2}}}^{x_{i+\frac{1}{2}}} \mathbf{A}(\mathbf{U}_i)\partial_x \mathbf{U}_i dx dt - \frac{\Delta t}{\Delta x}(\mathbf{D}_{i+\frac{1}{2}}^- + \mathbf{D}_{i-\frac{1}{2}}^+) \quad (10)$$

where i denotes the considered cell, n the current time level t^n, $\mathbf{U}_i^n$ and $\mathbf{U}_i^{n+1}$ the cell-averaged values of the conserved variable at time t^n and t^{n+1}, respectively, Δx the cell size, and Δt the time-step.

In a first order scheme, the integral term in Eq. (10) vanishes, since constant cell averaged values are assumed ($\partial_x \mathbf{U}_i = 0$) and the values at the cell interfaces correspond to the cell averaged values: $\mathbf{U}_{i+\frac{1}{2}}^+ \cong \mathbf{U}_{i+1}^n, \mathbf{U}_{i+\frac{1}{2}}^- \cong \mathbf{U}_i^n$.

The fluctuations (jump terms) $\mathbf{D}_{i+\frac{1}{2}}^-, \mathbf{D}_{i-\frac{1}{2}}^+$, which depend on the discontinuous values at the cell interface, are computed in the DOT Riemann solver as (Dumbser & Toro (2011)):

$$\mathbf{D}_{i+\frac{1}{2}}^{\pm} = \frac{1}{2}\int_0^1 \left[\mathbf{A}\left(\mathbf{\Psi}\left(s\right)\right) \pm \left|\mathbf{A}\left(\mathbf{\Psi}\left(s\right)\right)\right|\right] \frac{\partial \mathbf{\Psi}}{\partial s} ds \quad (11)$$

where the matrix $\mathbf{A}$ is defined according to Eq. (7) and the matrix absolute value $|\mathbf{A}|$ is evaluated as:

$$|\mathbf{A}| = \mathbf{R}|\Lambda|\mathbf{R}^{-1}, |\Lambda| = diag(|\lambda_1|, |\lambda_2|, |\lambda_3|, |\lambda_4|) \quad (12)$$

with $\mathbf{R}$ the matrix of the right eigenvectors of $\mathbf{A}$, $\mathbf{R}^{-1}$ its inverse, and $|\Lambda|$ the diagonal matrix of the eigenvalues absolute values.

The matrices $\mathbf{A}$ and $|\mathbf{A}|$ are evaluated along the path $\mathbf{\Psi}\left(s\right)$, that is a Lipschitz continuous function connecting the left ($\mathbf{U}_{i+\frac{1}{2}}^-$) and right ($\mathbf{U}_{i+\frac{1}{2}}^+$) states,

at the interface $i+\frac{1}{2}$, in phase-space. Particularly, the conserved variables appearing in matrices $\mathbf{A}$ and $|\mathbf{A}|$ are defined in the interval $s=[0;1]$ according to the following linear relation:

$$\mathbf{\Psi}(s)=\mathbf{U}^{-}_{i+\frac{1}{2}}+s(\mathbf{U}^{+}_{i+\frac{1}{2}}-\mathbf{U}^{-}_{i+\frac{1}{2}}) \tag{13}$$

Once $\mathbf{\Psi}(s)$, and then the matrices $\mathbf{A}$ and $|\mathbf{A}|$ are evaluated, the jump terms in Eq. (11) are computed by means of a G-point Gauss-Legendre quadrature rule (Dumbser & Toro (2011)) with positions s_j and weights ω_j in the interval [0;1]. Recalling that $\partial\mathbf{\Psi}/\partial s=\left(\mathbf{U}^{+}_{i+\frac{1}{2}}-\mathbf{U}^{-}_{i+\frac{1}{2}}\right)$, the approximated formula of Eq. (11) becomes:

$$\mathbf{D}^{\pm}_{i+\frac{1}{2}}\cong\frac{1}{2}\left\{\sum_{j=1}^{G}\omega_j\left[\mathbf{A}\left(\mathbf{\Psi}\left(s_j\right)\right)\pm\left|\mathbf{A}\left(\mathbf{\Psi}\left(s_j\right)\right)\right|\right]\right\}\left(\mathbf{U}^{+}_{i+\frac{1}{2}}-\mathbf{U}^{-}_{i+\frac{1}{2}}\right) \tag{14}$$

In this work, a three-point Gauss-Legendre quadrature, with the following positions and weights, is adopted:

$$s_1=\frac{5+\sqrt{15}}{10},\ s_2=\frac{1}{2},\ s_3=\frac{5-\sqrt{15}}{10},\ \omega_1=\frac{5}{18},\ \omega_2=\frac{8}{18},\ \omega_3=\frac{5}{18} \tag{15}$$

Apart from the DOT scheme, the velocity variable u, which is derived from the updated conserved variables as $u=\phi uh/\left(\phi\eta-\phi z\right)$, is here corrected in order to avoid the division by very small water depths as follows (Kurganov & Petrova (2007)):

$$u=\frac{\sqrt{2}h(uh)}{\sqrt{h^4+max(h^4,\varepsilon)}} \tag{16}$$

where ε is a small threshold ($\varepsilon=(\Delta x)^4$). The water depth and the specific discharge to be used in Eq. (16) are evaluated as $h=\phi\eta-\phi z$ and $uh=\phi uh/\phi$, respectively.

Finally, it is noteworthy that the absence of source terms in the set of the augmented governing equations (4), and the adoption of a finite volume scheme, automatically ensures the mass conservation (Hirsch (2007)).

5. Extension to high-order: the ADER scheme

The numerical scheme in Eq. (10) is extended to a second order of accuracy in both space and time by adopting the ADER approach (Toro et al. (2001), Titarev & Toro (2002), Toro & Titarev (2002)). The core of this technique is to use a space-time Taylor series expansion and a Cauchy-Kowalewski procedure in order to solve high-order Riemann problems at the element boundaries (Stecca et al. (2016)). Particularly, the ADER framework allows for the extension to high order in a one-step by adopting a temporal evolution of the spatial reconstructed polynomial present in each cell.

Reconstruction. The first step of the ADER approach is to compute a piecewise-linear reconstruction polynomial $\mathbf{p}_i$ of the conserved variables for each cell. Since a k-order accurate scheme requires a (k-1)-degree polynomial, a linear data reconstruction is sufficient for a second-order accurate scheme. Moreover, in order to avoid the occurrence of spurious oscillations near discontinuous solutions, a Total Variation Diminishing (TVD) scheme is considered (TVD schemes are frequently used for a second-order of accuracy). Therefore, the following first-order degree polynomial is adopted:

$$\mathbf{p}_i(x) = \mathbf{U}_i^n + \overline{\Delta}_i(x - x_i) \tag{17}$$

where $\overline{\Delta}_i$ is the limited reconstruction slope defined as (Toro (2013)):

$$\overline{\Delta}_i = \xi_i \Delta_i / \Delta x \tag{18}$$

with ξ_i and Δ_i denoting the slope limiter and the slope vector, respectively. This last term is evaluated as follows (Toro (2013)):

$$\Delta_i = \frac{1}{2}(1+\gamma)\,\Delta_{i-\frac{1}{2}} + \frac{1}{2}(1-\gamma)\,\Delta_{i+\frac{1}{2}} \tag{19}$$

with $\Delta_{i-\frac{1}{2}} = \mathbf{U}_i^n - \mathbf{U}_{i-1}^n$, $\Delta_{i+\frac{1}{2}} = \mathbf{U}_{i+1}^n - \mathbf{U}_i^n$ and γ is a free parameter in the interval $[-1, 1]$. In this work $\gamma = -1$ was adopted and thus $\Delta_i \equiv \Delta_{i+\frac{1}{2}}$.

Among the different formulations available for the slope limiter computation (Toro (2013)), the van Leer-type slope limiter is here adopted (Toro (2013)):

$$\xi(r) = \begin{cases} 0, & r \leq 0 \\ min\left\{\frac{2r}{1+r}, \xi_R(r)\right\}, & r > 0 \end{cases} \tag{20}$$

where terms r and $\xi_R(r)$ are defined as:

$$r = \frac{\Delta_{i-\frac{1}{2}}}{\Delta_{i+\frac{1}{2}}},\ \xi_R(r) = \frac{2\beta}{1-\gamma+(1+\gamma)r},\ \beta = \frac{2}{1-CFL} \tag{21}$$

with *CFL* the Courant-Friedrichs-Lewy number.

Space-time Taylor series expansion. The space-time evolution of each non-oscillatory polynomial, previously reconstructed at time t^n, is calculated according to the following first-order Taylor series expansion with respect to the barycentre x_i:

$$\mathbf{U}_i(x,t) \approx \mathbf{U}_i^n + (x-x_i)\partial_x\mathbf{U} + (t-t^n)\partial_t\mathbf{U} \tag{22}$$

The time derivative in Eq. (22) is calculated as a function of space derivative adopting the Cauchy-Kowaleski procedure that allows:

$$\partial_t\mathbf{U} = -\mathbf{A}\partial_x\mathbf{U} \tag{23}$$

Therefore, by substituting Eq. (23) in (22), the Taylor series expansion results:

$$\mathbf{U}_i(x,t) \approx \mathbf{U}_i^n + (x-x_i)\partial_x\mathbf{U} - \mathbf{A}(t-t^n)\partial_x\mathbf{U} \tag{24}$$

Finally, the variables expanded at each cell interfaces are evaluated by replacing the spatial derivatives in Eq. (24) with the derivative of the reconstruction polynomial (Eq. (17)):

$$\begin{aligned} \mathbf{U}^-_{i+\frac{1}{2}} &= \mathbf{U}^-_i(x_{i+\frac{1}{2}}, t^{n+\frac{1}{2}}) = \mathbf{U}_i^n + (\Delta x\mathbf{I} - \Delta t\mathbf{A})\,\tfrac{1}{2}\overline{\Delta}_i \\ \mathbf{U}^+_{i+\frac{1}{2}} &= \mathbf{U}^+_{i+1}(x_{i+\frac{1}{2}}, t^{n+\frac{1}{2}}) = \mathbf{U}_{i+1}^n - (\Delta x\mathbf{I} + \Delta t\mathbf{A})\,\tfrac{1}{2}\overline{\Delta}_i \end{aligned} \tag{25}$$

Update of the conserved variables. Dealing with the high-order extension of a numerical scheme that solves a non-conservative set of governing equations, the integral term in the explicit update formula (10) cannot be neglected due to

the presence of a not constant value inside each cell. Therefore, the space-time integral is approximated with a Gauss quadrature (Lee et al. (2013)):

$$\frac{1}{\Delta x}\int_{t^n}^{t^{n+1}}\int_{x_{i-\frac{1}{2}}}^{x_{i+\frac{1}{2}}}\mathbf{A}(\mathbf{U}_i)\partial_x\mathbf{U}_i dxdt \approx \frac{\Delta t}{\Delta x}\left(\sum_{j=1}^{G}\omega_j\mathbf{A}\left(\mathbf{\Psi}\left(\mathbf{U}^-_{i+\frac{1}{2}},\mathbf{U}^+_{i-\frac{1}{2}},s\right)\right)\right)\left(\mathbf{U}^+_{i+\frac{1}{2}}-\mathbf{U}^-_{i+\frac{1}{2}}\right) \tag{26}$$

The Taylor expansion previously described allows for the knowledge of the interface values in Eq. (25) that are then adopted to compute the integral term in Eq. (26) and the fluctuations in Eq. (14).
Finally, these quantities are introduced in the explicit formula in Eq. (10), and the update of the solution to the next time-step is performed.

6. *C-property*

The fulfillment of the *C-property* with a non-uniform porosity field and over a non-flat bottom is assessed in this section. Firstly, the water at rest condition is proved by showing that in this case the fluctuations in Eq. (14) are null.
Assuming a one-point Gauss-Legendre quadrature with weight $\omega = 1$ and position $s = 0.5$, and recalling that $u^-_{i+\frac{1}{2}} = u^+_{i+\frac{1}{2}} = 0$ and $\eta^-_{i+\frac{1}{2}} = \eta^+_{i+\frac{1}{2}} = \eta$, the path in Eq. (13) results:

$$\mathbf{\Psi}(0.5) = \begin{bmatrix} \frac{1}{2}\eta(\phi^+_{i+\frac{1}{2}}+\phi^-_{i+\frac{1}{2}}) \\ 0 \\ \frac{1}{2}(\phi^+_{i+\frac{1}{2}}+\phi^-_{i+\frac{1}{2}}) \\ \frac{1}{2}(z^+_{i+\frac{1}{2}}+z^-_{i+\frac{1}{2}}) \end{bmatrix} = \begin{bmatrix} \eta\overline{\phi} \\ 0 \\ \overline{\phi} \\ \overline{z} \end{bmatrix} \tag{27}$$

The conserved variables resulted from Eq. (27), which for sake of clarity have been marked with the overline symbol, are then used to compute the matrices $\mathbf{A}$ and $|\mathbf{A}|$. Particularly, the water surface elevation is evaluated from Eq. (27) as $\eta = \eta\overline{\phi}/\overline{\phi}$, and the water depth as $\overline{h} = \eta - \overline{z}$. Therefore, the matrices $\mathbf{A}$ and $|\mathbf{A}|$ are evaluated from Eq. (7) and (12), respectively, considering null velocity

and substituting the path values of Eq. (27):

$$\mathbf{A} = \begin{bmatrix} 0 & 1 & 0 & 0 \\ g\overline{h} & 0 & -g\eta^2 + g\eta\overline{z} & 0 \\ 0 & 0 & 0 & 0 \\ 0 & 0 & 0 & 0 \end{bmatrix} \quad |\mathbf{A}| = \begin{bmatrix} \sqrt{g\overline{h}} & 0 & -\eta\sqrt{g\overline{h}} & 0 \\ 0 & \sqrt{g\overline{h}} & 0 & 0 \\ 0 & 0 & 0 & 0 \\ 0 & 0 & 0 & 0 \end{bmatrix} \tag{28}$$

Finally, the fluctuations $\mathbf{D}^+_{i+\frac{1}{2}}$ and $\mathbf{D}^-_{i+\frac{1}{2}}$ become:

$$\begin{aligned} \mathbf{D}^+_{i+\frac{1}{2}} =& \frac{1}{2}\left[\mathbf{A}\left(\mathbf{\Psi}(s)\right) + |\mathbf{A}\left(\mathbf{\Psi}(s)\right)|\right]\left(\mathbf{U}^+_{i+\frac{1}{2}} - \mathbf{U}^-_{i+\frac{1}{2}}\right) \\ =& \frac{1}{2}\begin{bmatrix} \sqrt{g\overline{h}} & 1 & -\eta\sqrt{g\overline{h}} & 0 \\ g\overline{h} & \sqrt{g\overline{h}} & -g\eta^2 + g\eta\overline{z} & 0 \\ 0 & 0 & 0 & 0 \\ 0 & 0 & 0 & 0 \end{bmatrix}\begin{bmatrix} \eta(\phi^+_{i+\frac{1}{2}} - \phi^-_{i+\frac{1}{2}}) \\ 0 \\ \phi^+_{i+\frac{1}{2}} - \phi^-_{i+\frac{1}{2}} \\ z^+_{i+\frac{1}{2}} - z^-_{i+\frac{1}{2}} \end{bmatrix} \equiv \begin{bmatrix} 0 \\ 0 \\ 0 \\ 0 \end{bmatrix} \end{aligned} \tag{29}$$

$$\begin{aligned} \mathbf{D}^-_{i+\frac{1}{2}} =& \frac{1}{2}\left[\mathbf{A}\left(\mathbf{\Psi}(s)\right) - |\mathbf{A}\left(\mathbf{\Psi}(s)\right)|\right]\left(\mathbf{U}^+_{i+\frac{1}{2}} - \mathbf{U}^-_{i+\frac{1}{2}}\right) \\ =& \frac{1}{2}\begin{bmatrix} -\sqrt{g\overline{h}} & 1 & \eta\sqrt{g\overline{h}} & 0 \\ g\overline{h} & -\sqrt{g\overline{h}} & -g\eta^2 + g\eta\overline{z} & 0 \\ 0 & 0 & 0 & 0 \\ 0 & 0 & 0 & 0 \end{bmatrix}\begin{bmatrix} \eta(\phi^+_{i+\frac{1}{2}} - \phi^-_{i+\frac{1}{2}}) \\ 0 \\ \phi^+_{i+\frac{1}{2}} - \phi^-_{i+\frac{1}{2}} \\ z^+_{i+\frac{1}{2}} - z^-_{i+\frac{1}{2}} \end{bmatrix} \equiv \begin{bmatrix} 0 \\ 0 \\ 0 \\ 0 \end{bmatrix} \end{aligned} \tag{30}$$

After having proved that the jump terms are null, and hence the derived DOT Riemann solver theoretically guaranties the quiescent flow condition, the exact *C-property* preservation is numerically verified. Following Xing & Shu (2005), the bottom topography z is described in the range $0 \leq x \leq 10$ by both a smooth function:

$$z(x) = 5e^{-\frac{2}{5}(x-5)^2} \tag{31}$$

and a discontinuos function:

$$z(x) = \begin{cases} 4 & 4 \leq x \leq 8 \\ 0 & otherwise \end{cases} \tag{32}$$

As initial condition of the two bottom configurations, a constant free-surface elevation $\eta = z + h = 10$ m is assumed. The domain is discretized with N= 500 computational cells and the solution is computed until t=0.5 s. Additionally, the original test case has been here modified by including a variable porosity field: in order to test the presence of discontinuities, a random porosity field in the range [0,1] is considered. The setup of these tests is shown in Fig. 1a and Fig. 1b for the smooth and discontinuous bottom, respectively.

The presence of wet and dry interfaces has been also tested by considering the smooth bottom and a free-surface elevation $\eta = 3$ m (Fig. 1c).

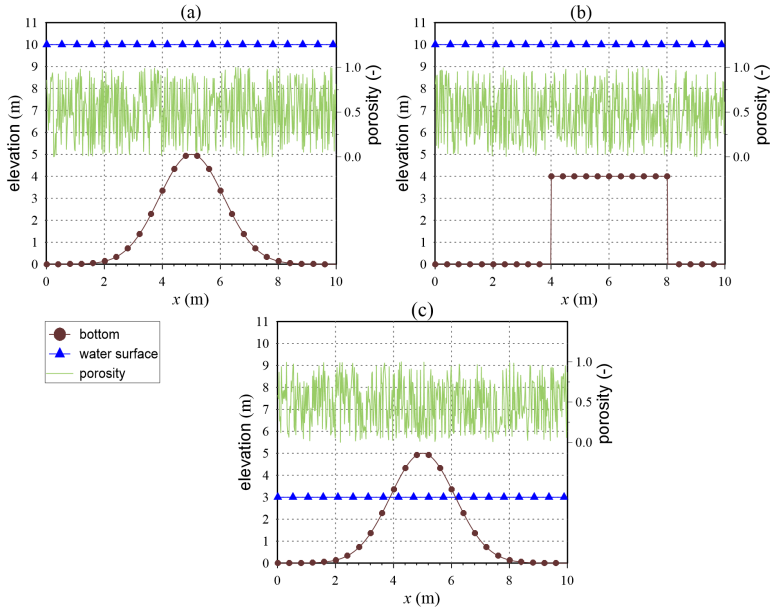

Figure 1: *C-property* verification: stationary flow with a non-uniform porosity over a smooth (a) and discontinuous (b) bottom, and (c) containing wet and dry interfaces.

For both water surface elevation and specific discharge variables, the L_1 and L_∞ error norms were computed in order to quantify the misfit between the numerical and the exact/initial solution. Table 1 shows that the *C-property* is exactly preserved up to the machine precision.

Table 1: *C-property* verification: L_1 and L_∞ errors for water surface elevation and specific discharge

Bottom	$L_1(\eta)$	$L_1(uh)$	$L_\infty(\eta)$	$L_\infty(uh)$
(a) smooth	3.34E-16	4.36E-13	1.78E-15	4.57E-11
(b) discontinuos	3.27E-16	4.38E-13	1.78E-15	3.82E-11
(c) wet and dry	4.16E-08	2.19E-13	1.77E-07	9.24E-11

7. Numerical results

In this section, the order of accuracy is firstly verified and then the numerical model is validated performing some Riemann problems characterized by bottom or porosity discontinuities.

7.1. ***Convergence***

The second order of accuracy of the implemented numerical scheme is verified by performing the following quasi-stationary test (LeVeque (1998)), where the bottom topography (Fig. 2) presents a bump that is described as:

$$z(x) = \begin{cases} 0.25(\cos(10\pi(x-1.5))+1) & if 1.4 \leq x \leq 1.6 \\ 0 & otherwise \end{cases} \tag{33}$$

At the beginning of the test the flow is at rest with the water surface elevation shown in Fig. 2 and described as:

$$\eta(x) = \begin{cases} 1.2 & if 1.1 \leq x \leq 1.2 \\ 1 & otherwise \end{cases} \tag{34}$$

The simulation is carried on until time $t = 0.2$ s, when the water pulse traveling downstream has already overstepped the bump. At this time, the water surface elevation and the specific discharge are as shown in Fig. 3 (a) and (b), respectively.

As numerical reference solution for testing the order of accuracy, a very fine mesh discretizing the domain with $N = 3200$ cells was adopted. Meanwhile, the

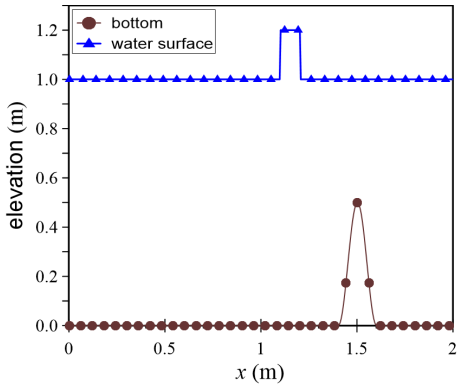

Figure 2: Convergence analysis: bottom and initial water surface elevation.

remaining simulations were performed with coarser meshes from $N = 100$ up to $N = 800$ cells. In Fig. 3, the reference solution and the one obtained with $N = 200$ cells are shown. No spurious oscillations arise, thus confirming, that the proposed scheme is capable of accurately reproducing the perturbation of a quiescent state over a smooth bottom.

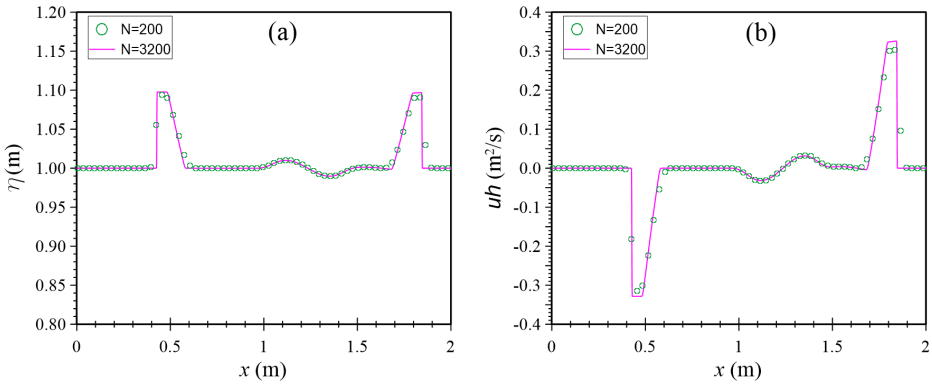

Figure 3: Convergence analysis: water surface elevation (a) and specific discharge (b) at time $t = 0.2$ s, simulated with 200 and 3200 cells.

The error norms L_1 and L_2 computed for both water surface elevation and specific discharge, and reported in Table 2, confirm that the scheme guarantees a second order of accuracy.

Table 2: Convergence: number of cells N, error norms L_1 and L_2, and order of accuracy for water surface elevation and specific discharge.

N	$L_1(\eta)$	$O(L_1(\eta))$	$L_2(\eta)$	$O(L_2(\eta))$	$L_1(uh)$	$O(L_1(uh))$	$L_2(uh)$	$O(L_2(uh))$
100	1.61E-02		1.61E-02		5.70E-02		5.71E-02	
200	4.20E-03	1.94	4.24E-03	1.93	1.50E-02	1.93	1.51E-02	1.92
400	1.00E-03	2.07	1.12E-03	1.92	3.69E-03	2.02	4.05E-03	1.90
800	2.39E-04	2.06	2.70E-04	2.05	8.86E-04	2.06	1.02E-03	1.99

*7.2. **Riemann Problems***

The capability of the proposed numerical scheme to reproduce some Riemann problems characterized by discontinuities is investigated in this section. The exact solutions used to compare the numerical results are obtained by means of the Exact Riemann solvers *ad-hoc* derived to treat porosity (Ferrari et al. (2017)) and bottom (Rosatti & Begnudelli (2010)) discontinuities, respectively. In all the tests, the domain is 100 m long and discretized with N=600 cells, and the discontinuity in the initial values is located at $x = 50$ m.
In order to test different wave configurations, the initial conditions reported in Table 3 are considered.

Table 3: Initial conditions of the Riemann problems.

Test number	ID	$h_L(m)$	$u_L(m/s)$	$\phi_L(-)$	$z_L(m)$	$h_R(m)$	$u_R(m/s)$	$\phi_R(-)$	$z_R(m)$
1	RPS	8	0	0.9	0	3	0	0.7	0
2	RPR	8	-2	0.9	0	6.5	5	0.7	0
3	RRPR	6	-18	0.9	0	15	0	0.7	0
4	RBS	5	0	1	0	1	0	1	0.5
5	RBR	8	-2	1	0	5	7	1	0.5
6	RRBR	6	-16	1	0	10	0	1	0.5
7	RB	4	0	1	0	0	0	1	1

The first test, Rarefaction-Porosity-Shock (RPS), is a Stoker Riemann problem, which at $t = 0$ presents still water with different depths at both sides of $x = 50$ m, where a porosity discontinuity is located. The "dam-break" generates a left rarefaction propagating to the left of the porous discontinuity, a stationary step at $x = 50$ m and a shock wave at the right. Figure 4 shows that the numerical results obtained with both first and second order accurate schemes

well agree with the exact solution, both for water depth and velocity.

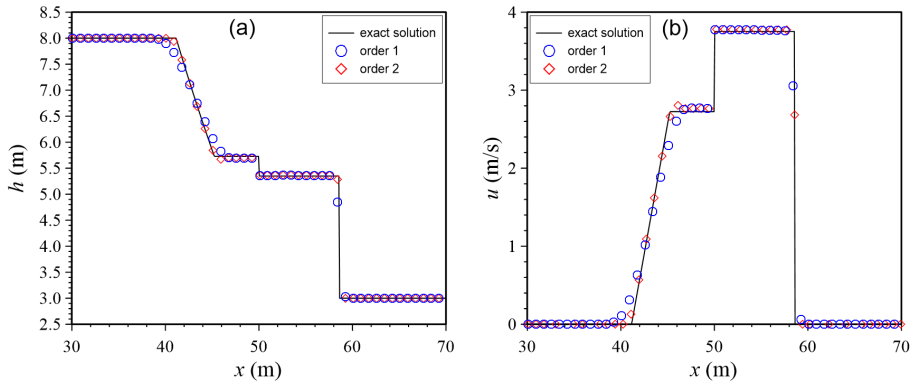

Figure 4: RPS test at $t = 1s$: water depth (a) and velocity (b) comparison between exact and numerical solutions.

In the second Riemann problem, Rarefaction-Porosity-Rarefaction (RPR), two rarefactions origin from the discontinuity, one left-moving and the other right-going. The comparison showed in Fig. 5 highlights that the numerical scheme well captures the wave pattern and the intermediate state values of this divergent flow.

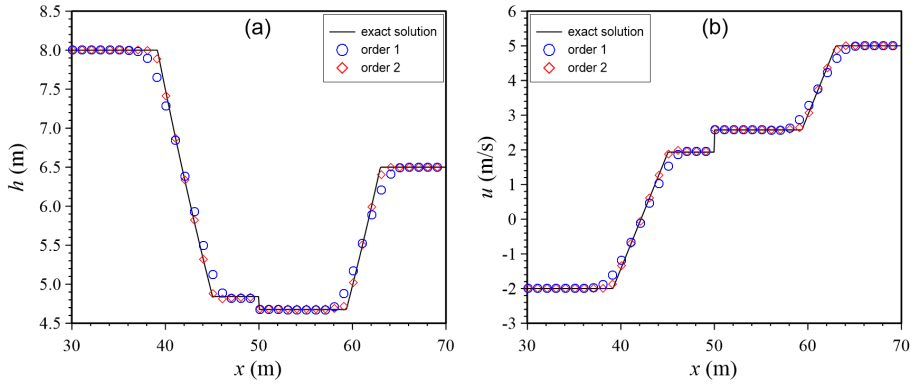

Figure 5: RPR test at $t = 1s$: water depth (a) and velocity (b) comparison between exact and numerical solutions.

As pointed out in the Introduction, one of the main advantages of the DOT Riemann solver is to be entropy-satisfying, that means that it does not require

any special procedure (e.g. the solution of non-linear system of equations in the Roe solvers), to ensure the Lax entropy condition also in the presence of transonic rarefactions. Therefore, the third Riemann problem, Rarefaction-Rarefaction-Porosity-Rarefaction (RRPR), concerns the passage through the critical state at the discontinuity location. Two rarefactions depart at the left of the middle contact wave, one left-going and the other right-facing, meanwhile at the right of the discontinuity a right rarefaction develops. The numerical model is capable of capturing the wave configurations, even if the right intermediate state of this severe test is slightly underestimated (Fig. 6).

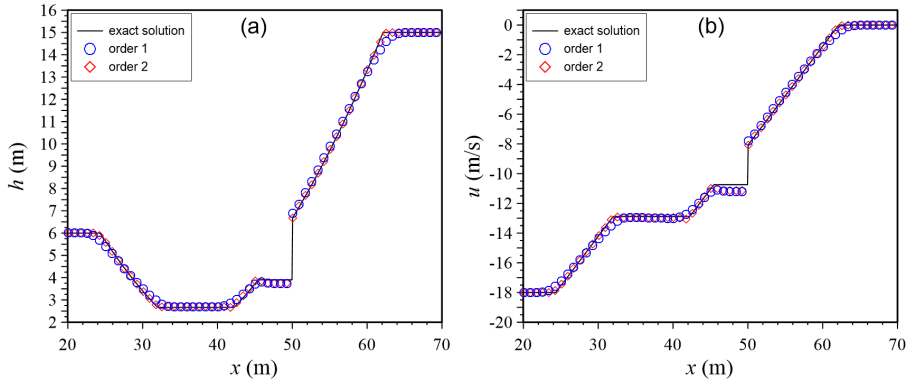

Figure 6: RRPR test at $t = 1s$: water depth (a) and velocity (b) comparison between exact and numerical solutions.

In the following, the numerical model is tested considering at $x = 50$ m a bottom step instead of a porous discontinuity: this bed-step generates the three wave configurations previously described. Figures 7, 8 and 9 display the results at time $t = 1$ s for the Rarefaction-Bottom-Shock (RBS), Rarefaction-Bottom-Rarefaction (RBR), and Rarefaction-Rarefaction-Bottom-Rarefaction (RRBR) test, respectively. In all the tests, the numerical model well agree with the exact solver: the contact wave across which the bed elevation varies is captured, as well as the wave pattern and the intermediate values.

The last tested configuration (RB) presents a still column of water collapsing on a dry bed step at right. Figure 10 compares the numerical solution at time

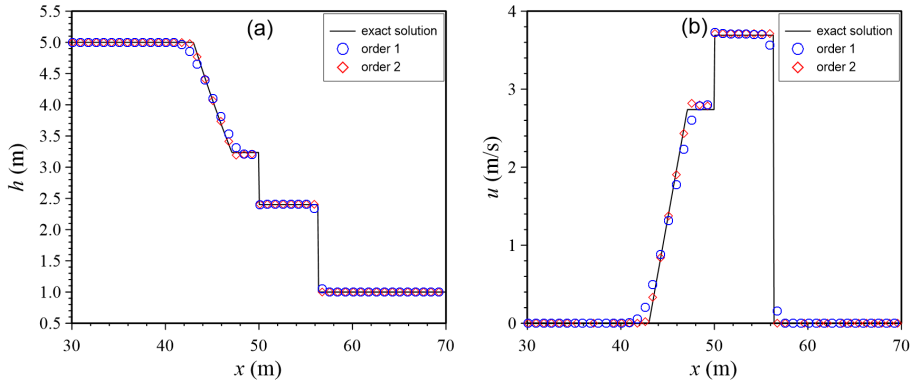

Figure 7: RBS test at $t = 1s$: water depth (a) and velocity (b) comparison between exact and numerical solutions.

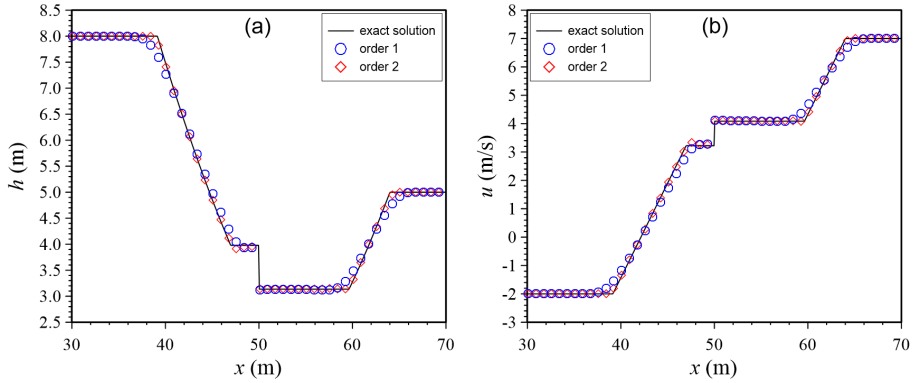

Figure 8: RBR test at $t = 1s$: water depth (a) and velocity (b) comparison between exact and numerical solutions.

$t = 0.4$ s with the exact solution presented in Han & Warnecke (2014). Both order of accuracy well reproduce the rarefaction wave travelling at the left side of the step and the dry bed state at right; as expected the results of the second order scheme better approximate the wave on the dry bed (Figure 10b).

8. Conclusions and future work

This work focused on the derivation of a new well-balanced numerical scheme capable of treating discontinuities in the framework of the Shallow Water Equa-

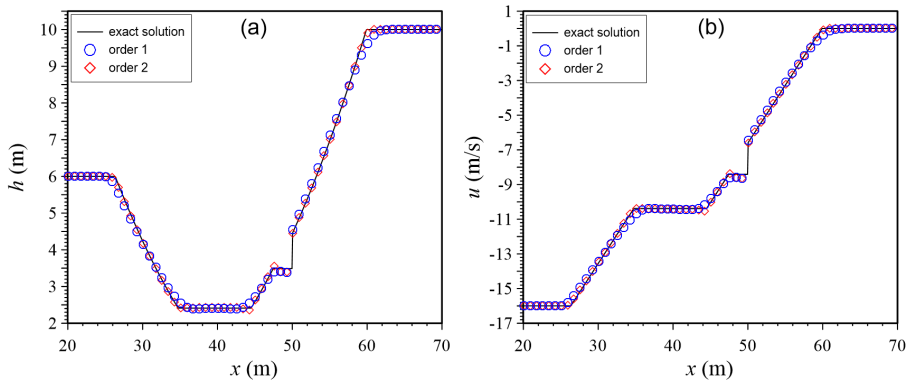

Figure 9: RRBR test at $t = 1s$: water depth (a) and velocity (b) comparison between exact and numerical solutions.

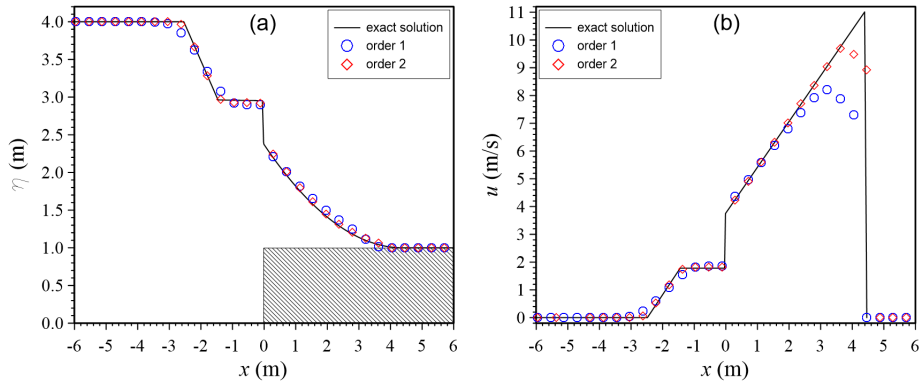

Figure 10: RB test at $t = 0.4s$: water surface elevation (a) and velocity (b) comparison between exact and numerical solutions.

tions with porosity. To this purpose, an augmented Riemann solver accounting for both porosity and bottom non-conservative products has been introduced and its eigenstructure has been studied. Moreover, an entropy-satisfying DOT Riemann solver, which strictly conserves mass, has been developed and the numerical scheme has been then extended to high-order in the ADER framework. As confirmed by the convergence analysis, a second-order of accuracy based on the TVD reconstruction has been achieved, and higher order can be addressed in the future.

As theoretically and numerically verified, the numerical model preserves the

exact *C-property* over a non-flat bottom and with a discontinuous porosity field. Finally, the numerical model has been validated against a selection of Riemann problems, including also transonic waves and wet and dry fronts.

The investigation of the influence of the integration path on the numerical solver (Caleffi & Valiani (2017)), the extension of the 1D proposed numerical model to two dimensions, and the application to real test cases are left to future works.

References

Abgrall, R., & Karni, S. (2010). A comment on the computation of non-conservative products. *Journal of Computational Physics*, *229*, 2759–2763. URL: `http://dx.doi.org/10.1016/j.jcp.2009.12.015`. doi:`10.1016/j.jcp.2009.12.015`.

Benkhaldoun, F., Elmahi, I., Moumna, A., & Seaid, M. (2016). A non-homogeneous riemann solver for shallow water equations in porous media. *Applicable Analysis*, *95*, 2181–2202.

Bernetti, R., Titarev, V. A., & Toro, E. F. (2008). Exact solution of the riemann problem for the shallow water equations with discontinuous bottom geometry. *Journal of Computational Physics*, *227*, 3212–3243.

Bruwier, M., Archambeau, P., Erpicum, S., Pirotton, M., & Dewals, B. (2017). Shallow-water models with anisotropic porosity and merging for flood modelling on cartesian grids. *Journal of hydrology*, *554*, 693–709.

Caleffi, V., & Valiani, A. (2017). Well balancing of the swe schemes for moving-water steady flows. *Journal of Computational Physics*, *342*, 85–116.

Caleffi, V., Valiani, A., & Li, G. (2016). A comparison between bottom-discontinuity numerical treatments in the dg framework. *Applied Mathematical Modelling*, *40*, 7516–7531.

Canestrelli, A., Siviglia, A., Dumbser, M., & Toro, E. F. (2009). Well-balanced high-order centred schemes for non-conservative hyperbolic systems. applications to shallow water equations with fixed and mobile bed. *Advances in Water Resources*, *32*, 834–844.

Castro, M., Gallardo, J., & Parés, C. (2006). High order finite volume schemes based on reconstruction of states for solving hyperbolic systems with non-conservative products. applications to shallow-water systems. *Mathematics of computation*, *75*, 1103–1134.

Castro, M. J., Pardo Milanés, A., & Parés, C. (2007). Well-balanced numerical schemes based on a generalized hydrostatic reconstruction technique. *Mathematical Models and Methods in Applied Sciences*, *17*, 2055–2113.

Cea, L., & Vázquez-Cendón, M. E. (2010). Unstructured finite volume discretization of two-dimensional depth-averaged shallow water equations with porosity. *International Journal for Numerical Methods in Fluids*, *63*, 903–930.

Cozzolino, L., Della Morte, R., Covelli, C., Del Giudice, G., & Pianese, D. (2011). Numerical solution of the discontinuous-bottom shallow-water equations with hydrostatic pressure distribution at the step. *Advances in water resources*, *34*, 1413–1426.

Cozzolino, L., Pepe, V., Cimorelli, L., D'Aniello, A., Della Morte, R., & Pianese, D. (2018). The solution of the dam-break problem in the porous shallow water equations. *Advances in water resources*, *114*, 83–101.

Dal Maso, G., Le Floch, P., & Murat, F. (1995). Definition and weak stability of nonconservative products. *Journal de mathématiques pures et appliquées*, *74*, 483–548.

Defina, A., D'Alpaos, L., & Matticchio, B. (1994). New set of equations for very shallow water and partially dry areas suitable to 2d numerical models. (pp. 72–81). URL: `https://www.scopus.com/inward/record.uri?eid=2-s2.`

0-0027961472&partnerID=40&md5=0d5fc837bb1b9019907088da25d41015 cited By 47.

Dumbser, M., & Toro, E. F. (2011). A simple extension of the osher riemann solver to non-conservative hyperbolic systems. *Journal of Scientific Computing*, *48*, 70–88.

Ferrari, A., Vacondio, R., Dazzi, S., & Mignosa, P. (2017). A 1d–2d shallow water equations solver for discontinuous porosity field based on a generalized riemann problem. *Advances in water resources*, *107*, 233–249.

Ferrari, A., Viero, D. P., Vacondio, R., Defina, A., & Mignosa, P. (2019). Flood inundation modeling in urbanized areas: A mesh-independent porosity approach with anisotropic friction. *Advances in water resources*, *125*, 98–113.

Finaud-Guyot, P., Delenne, C., Lhomme, J., Guinot, V., & Llovel, C. (2010). An approximate-state riemann solver for the two-dimensional shallow water equations with porosity. *International Journal for Numerical Methods in Fluids*, *62*, 1299–1331.

George, D. L. (2008). Augmented riemann solvers for the shallow water equations over variable topography with steady states and inundation. *Journal of Computational Physics*, *227*, 3089–3113.

Guinot, V., Delenne, C., Rousseau, A., & Boutron, O. (2018). Flux closures and source term models for shallow water models with depth-dependent integral porosity. *Advances in water resources*, *122*, 1–26.

Guinot, V., Sanders, B. F., & Schubert, J. E. (2017). Dual integral porosity shallow water model for urban flood modelling. *Advances in water resources*, *103*, 16–31.

Guinot, V., & Soares-Frazão, S. (2006). Flux and source term discretization in two-dimensional shallow water models with porosity on unstructured grids. *International Journal for Numerical Methods in Fluids*, *50*, 309–345.

Han, E., & Warnecke, G. (2014). Exact riemann solutions to shallow water equations. *Quarterly of Applied Mathematics*, (pp. 407–453).

Hirsch, C. (2007). *Numerical computation of internal and external flows: The fundamentals of computational fluid dynamics*. Elsevier.

Kurganov, A., & Petrova, G. (2007). A second-order well-balanced positivity preserving central-upwind scheme for the saint-venant system. *Communications in Mathematical Sciences*, *5*, 133–160.

Lee, B. J., Toro, E. F., Castro, C. E., & Nikiforakis, N. (2013). Adaptive osher-type scheme for the euler equations with highly nonlinear equations of state. *Journal of Computational Physics*, *246*, 165–183.

LeRoux, A. (1998). Discrétisation des termes sources raides dans les problemes hyperboliques. *Systemes hyperboliques: noveau schemas et nouvelles applications. Ecoles CEA-EDFINRIA problemes non linéaires appliqués, INRIA Rocquencourt (France)*, .

LeVeque, R. J. (1998). Balancing source terms and flux gradients in high-resolution godunov methods: the quasi-steady wave-propagation algorithm. *Journal of computational physics*, *146*, 346–365.

Liang, Q., & Borthwick, A. G. (2009). Adaptive quadtree simulation of shallow flows with wet–dry fronts over complex topography. *Computers & Fluids*, *38*, 221–234.

Murillo, J., & García-Navarro, P. (2010). Weak solutions for partial differential equations with source terms: Application to the shallow water equations. *Journal of Computational Physics*, *229*, 4327–4368.

Murillo, J., & García-Navarro, P. (2012). Augmented versions of the hll and hllc riemann solvers including source terms in one and two dimensions for shallow flow applications. *Journal of Computational Physics*, *231*, 6861–6906.

Navas-Montilla, A., & Murillo, J. (2015). Energy balanced numerical schemes with very high order. the augmented roe flux ader scheme. application to the shallow water equations. *Journal of Computational Physics*, *290*, 188–218.

Osher, S., & Solomon, F. (1982). Upwind difference schemes for hyperbolic systems of conservation laws. *Mathematics of computation*, *38*, 339–374.

Özgen, I., Liang, D., & Hinkelmann, R. (2016a). Shallow water equations with depth-dependent anisotropic porosity for subgrid-scale topography. *Applied Mathematical Modelling*, *40*, 7447–7473.

Özgen, I., Zhao, J., Liang, D., & Hinkelmann, R. (2016b). Urban flood modeling using shallow water equations with depth-dependent anisotropic porosity. *Journal of Hydrology*, *541*, 1165–1184.

Parés, C. (2006). Numerical methods for nonconservative hyperbolic systems: a theoretical framework. *SIAM Journal on Numerical Analysis*, *44*, 300–321.

Rosatti, G., & Begnudelli, L. (2010). The riemann problem for the one-dimensional, free-surface shallow water equations with a bed step: Theoretical analysis and numerical simulations. *Journal of Computational Physics*, *229*, 760–787.

Sanders, B. F., Schubert, J. E., & Gallegos, H. A. (2008). Integral formulation of shallow-water equations with anisotropic porosity for urban flood modeling. *Journal of hydrology*, *362*, 19–38.

Soares-Frazão, S., Lhomme, J., Guinot, V., & Zech, Y. (2008). Two-dimensional shallow-water model with porosity for urban flood modelling. *Journal of Hydraulic Research*, *46*, 45–64.

Stecca, G., Siviglia, A., & Blom, A. (2016). An accurate numerical solution to the saint-venant-hirano model for mixed-sediment morphodynamics in rivers. *Advances in water resources*, *93*, 39–61.

Titarev, V. A., & Toro, E. F. (2002). Ader: Arbitrary high order godunov approach. *Journal of Scientific Computing*, *17*, 609–618.

Toro, E., Millington, R., & Nejad, L. (2001). Towards very high order godunov schemes. In *Godunov methods* (pp. 907–940). Springer.

Toro, E., & Titarev, V. (2002). Solution of the generalized riemann problem for advection–reaction equations. *Proceedings of the Royal Society of London. Series A: Mathematical, Physical and Engineering Sciences*, *458*, 271–281.

Toro, E. F. (2001). *Shock-capturing methods for free-surface shallow flows*. John Wiley.

Toro, E. F. (2013). *Riemann solvers and numerical methods for fluid dynamics: a practical introduction*. Springer Science & Business Media.

Velickovic, M., Zech, Y., & Soares-Frazão, S. (2017). Steady-flow experiments in urban areas and anisotropic porosity model. *Journal of Hydraulic Research*, *55*, 85–100.

Viero, D. P. (2019). Modelling urban floods using a finite element staggered scheme with an anisotropic dual porosity model. *Journal of hydrology*, *568*, 247–259.

Xing, Y., & Shu, C.-W. (2005). High order finite difference weno schemes with the exact conservation property for the shallow water equations. *Journal of Computational Physics*, *208*, 206–227.